RSC Advances

PAPER

View Article Online
View Journal | View Issue

Cite this: *RSC Adv.*, 2022, **12**, 1653

Enhanced thermoelectric performance in Sb–Br codoped Bi_2Se_3 with complex electronic structure and chemical bond softening†

Ju Zhang, Shiqi Zhong and San-Huang Ke*

Prior experimental work showed that Bi_2Se_3, as a sister compound of the best room-temperature thermoelectric material Bi_2Te_3, has remarkably improved thermoelectric performance by Sb–Br codoping. But the relationship between its crystalline structure and thermoelectric properties is still unclear to date. Here, we use first-principles calculations to explore the possible reasons for such improvement. The electronic structures of $Bi_{2-x}Sb_x(Se_{1-y}Br_y)_3$ ($x = 0, 1, 2$; $y = 0, 0.08$) are systematically investigated. Significant effects of 8% Br codoping in $BiSbSe_3$ are found. First, the Br atom acts as an electron donor, thus greatly increasing the carrier concentration. Second, similar to the effect of Sb doping, Br codoping further improves greatly the degeneracy of the conduction band edge, which leads to a remarkably increased density-of-states effective mass without deterioration of the carrier mobility, and simultaneously preserves a large Seebeck coefficient of ~ -254 μV K^{-1} at 800 K. In addition, the Br codoping softens the chemical bonds, which enhances anharmonic scattering and further reduces the lattice thermal conductivity. We predict that the maximum zT of $BiSb(Se_{0.92}Br_{0.08})_3$ at 800 K can reach 0.96 with the carrier concentration of 9.22×10^{19} cm^{-3}. This study rationalizes a potential strategy to improve the thermoelectric performance of Bi_2Se_3-based thermoelectric materials.

Received 30th November 2021
Accepted 29th December 2021

DOI: 10.1039/d1ra08726f

rsc.li/rsc-advances

Introduction

With about two-thirds of the world's produced energy being lost as waste heat,[1] thermoelectric (TE) materials which can directly convert exhaust heat into usable electricity have been investigated widely as clean and sustainable energy materials.[2] The TE performance depends on the dimensionless figure of merit $zT = S^2\sigma T/\kappa$, where S, σ, κ, and T are the Seebeck coefficient, electrical conductivity, total thermal conductivity (including the lattice contribution κ_L and carrier contribution κ_e), and absolute temperature, respectively.[3–5] An excellent TE material requires a high value of zT simultaneously with a high power factor (PF = $S^2\sigma$) and a low κ.[6,7] Because of the strong coupling between S, σ, and κ_e, it is very difficult to enhance zT by optimizing only one of these parameters.[8] To date, decoupling of these electronic parameters by band engineering approaches through increasing the number of effective energy valley and minimizing κ_L (the only independent parameter) have proved to be effective strategies for enhancing zT.[9]

It is well known that the electrical transport properties of a material are dominated by the details of its band structure and scattering mechanism. The optimized electrical transport properties of a thermoelectric material depend on the weighted mobility,[10] $\mu(m^*_{DOS}/m_e)^{3/2}$, here μ, m^*_{DOS} and m_e are the mobility of carriers, density-of-states (DOS) effective mass and electron mass, respectively. The DOS effective mass is given as[11] $m^*_{DOS} = N_v^{2/3}m^*_b$, where N_v is the band degeneracy and m^*_b is the band effective mass. Actually, for the charge carriers predominantly scattered by acoustic phonons, the mobility is expected that $\mu \propto 1/m^{*5/2}_b$.[12] Consequently, increasing the m^*_b should be detrimental to the thermoelectric performance. In contrast, the convergence of many charge carrying valleys has virtually no detrimental effects. Therefore, multiple degenerate valleys are generally desired, thanks to the separate pockets of Fermi surface with the same energy, which have the effect of producing large m^*_{DOS} without explicitly increasing m^*_b. Besides, materials with soft chemical bonds and anharmonic lattice dynamics would suppress the lattice thermal conductivity.[1,13,14] However, the combination of all these features has been identified[12,15] with a large challenge in achieving high-performance thermoelectrics through an avenue simultaneously possessing large band degeneracy and strong anharmonic lattice dynamics, which are highly inter-dependent. As the best commercialized thermoelectric material found so far, Bi_2Te_3 has excellent σ, S, and large zT (for both n-type and p-type), and therefore have been widely applied for TE power generation and electronic cooling around room temperature.[16] However, Te is a scarce element in the crust of the earth and its cost would rise

MOE Key Laboratory of Microstructured Materials, School of Physics Science and Engineering, Tongji University, 1239 Siping Road, Shanghai 200092, China. E-mail: shke@tongji.edu.cn

† Electronic supplementary information (ESI) available. See DOI: 10.1039/d1ra08726f

sharply along with large-scale applications. Therefore, Te-free TE materials have attracted great attention.

As an important low-cost thermoelectric material, Bi_2Se_3, a sister compound of Bi_2Te_3, has also been receiving attention due to the constituent of abundant elements. Specifically, it possesses the same layered structure and the weak inter-layer van der Waals bonding, which makes it easier to be separated into plates.[17] Smaller plates with more interfaces mean lower κ_L theoretically, which is very favorable to thermoelectric applications. However, Bi_2Se_3 has drawn little attention owing to its relatively poor TE performance with zT being $\sim$0.4.[18] Many efforts have been focused on optimizing the TE merit value of Bi_2Se_3 in recent years. Liu *et al.* demonstrated that the key limitations for the zT of Bi_2Se_3 are its poor electrical transport properties and high κ.[18,19] With the intrinsically small band gap (E_g) $\sim$ 0.3 eV and low carrier concentration (n), Bi_2Se_3 displays bipolar effect.[20] The excitation of minor carriers attenuates the S, while the κ_e is enhanced at the same time, suggesting a small PF and a high κ_e.[21] Shakouri *et al.* proposed that enlarging the band gap would be an effective method to avoid bipolar conduction.[57] Increasing n directly is another adequate means to minify the effects of minority carriers. In addition, the single valley of conduction band minimum (CBM) ($N_v = 1$) will lead to a low DOS and also a small power factor for n-type Bi_2Se_3.[22] In the meantime, suppression of phonon transport is also critical to largely enhance the zT of Bi_2Se_3. Recently, Zhao *et al.* successfully introduced Sb–Br into the intrinsic semiconductor Bi_2Se_3 and obtained a maximum zT of 1.4 for n-type $BiSb(Se_{0.94}Br_{0.06})_3$ at 800 K. That is analogous to the most n-type Te-free TE materials, indicating that Sb–Br codoping is an effective approach in improving TE properties of Bi_2Se_3 alloy compounds. They found that Sb doping reduced κ on account of strong anharmonicity and soft bonds.[23] But the electrical transport properties of $BiSbSe_3$ is still poor because of the extremely low n and the imbalance between the effective mass and n. Then, *via* heavy Br-doping in $BiSbSe_3$, Liu *et al.* acquired a high n and further optimized TE properties. Although there is a computational work about the electronic structure of $BiSbSe_3$ alloy[22] and a parameterized model theoretical analysis about the effects of Br doping,[23] the detailed physical reasons in atomic level for Br codoping to further significantly improve TE properties have not been investigated yet. Particularly, the relationship between the crystalline atomic structure and the TE performance for $Bi_{2-x}Sb_x(Se_{1-y}Br_y)_3$ (x = 0, 1, 2; y = 0, 0.08) is still unclear so far.

In this work, we report a systematic first-principles study on the TE properties of the $Bi_{2-x}Sb_x(Se_{1-y}Br_y)_3$ (x = 0, 1, 2; y = 0, 0.08) alloy. The calculations are based on the density functional theory (DFT) for the atomic and electronic structures and based on the Boltzmann transport theory for the electron and phonon transport processes. It has been shown in literature that DFT is one of the most common and successful theoretical tools for probing TE materials, such as $Cu_{12}Sb_4S_{13}$.[56] x = 0, 1 in the $Bi_{2-x}Sb_xSe_3$ system is identified to be the transition boundary of the rhombohedral structure and orthorhombic structure. The strong hybridization between Sb and Se atoms in the complex crystal structure of orthorhombic $BiSbSe_3$ with alloying 50% Sb on Bi sites makes it have a lower κ_L. In addition, the increase of structural symmetry is helpful to obtain a large energy valley degeneracy (N_v), and a large σ can be achieved by increasing conductive channels. The N_v and chemical bond softening can be further improved significantly by codoping 8% Br at Se sites. The improved N_v will enhance the m^*_{DOS} without reducing the μ. The further softened phonons are beneficial to enhancing anharmonic scattering and further decrease the κ_L. The Br codoping also moves the Fermi level (E_F) into the conduction band (CB), resulting in a significant increase of n and σ. Interestingly, the increase of n does not reduce largely S because of the increased m^*_{DOS}. Eventually, a peak zT value of $\sim$0.96 at 800 K can be realized in n-type alloy compounds $BiSb(Se_{0.92}Br_{0.08})_3$ with the carrier concentration of 9.22×10^{19} cm^{-3}.

Results and discussion

Crystal structure and electronic structure

Bi_2Se_3 compound has a rhombohedral crystal structure with space group $D^5_{3d}(R\bar{3}m)$ no. 166 (Fig. 1(a)). In order to generate a reliable atomic structure for this compound, we first optimized its crystal structure with PBE functional as implemented in VASP in the total energy method. Its lattice constants a, b and c are found to be 4.19, 4.19 and 30.8 Å, respectively, which are in good agreement with the experimental values 4.14, 4.14 and 28.63 Å,[27] proving the reliability of our theoretical modeling. The distinct layered structure consists of a regular octahedron structure with Bi atom as the center and Se atom as the vertex. On the other hand, Sb_2Se_3 exhibits an orthorhombic structure composed of a tetragonal conical pentahedron with Sb as the bottom center and Se as the vertex, as shown in Fig. 1(b). According to the previous results of Zhao *et al.*,[23] the substitution of Sb for 50% Bi atoms in Bi_2Se_3 will induce a phase transition from the rhombohedral structure to the orthorhombic structure. Therefore, we utilize Bi atoms to replace the two nonequivalent sites of Sb1 atom in Sb_2Se_3, and adopt a structure with the lower energy to simulate the $BiSbSe_3$. It displays a significant chain-like structure of orthorhombic phase by forming an octahedral structure with Bi atom as the center and Se atom as the vertex, and a triangular pyramidal tetrahedron with Sb and three Se atoms as the vertex is also formed (Fig. 1(c)).

This complex crystal structure of $BiSbSe_3$ is favorable to reducing the κ_L because of the structural phase transition and the formation of the chain-like structure. Since the structural rhombohedral–orthorhombic phase transition is related to the breakage of part of the cation–anion bonds, half of the octahedral coordination cations are converted to five coordination, as reported previously by Yang *et al.*[22] Finally, we consider the possible substitution of single Br atom for Se. There are three nonequivalent sites of Se atom in $BiSbSe_3$, therefore, three possible structures can be formed. It is found by calculation that the total energies per cell of the three structures are −78.373, −78.285 and −78.308 eV, respectively. Furthermore, we calculate the energy band structures and thermoelectric transport properties for the three structures, respectively. The results are compared in Fig. S1 and S2,† which show that the

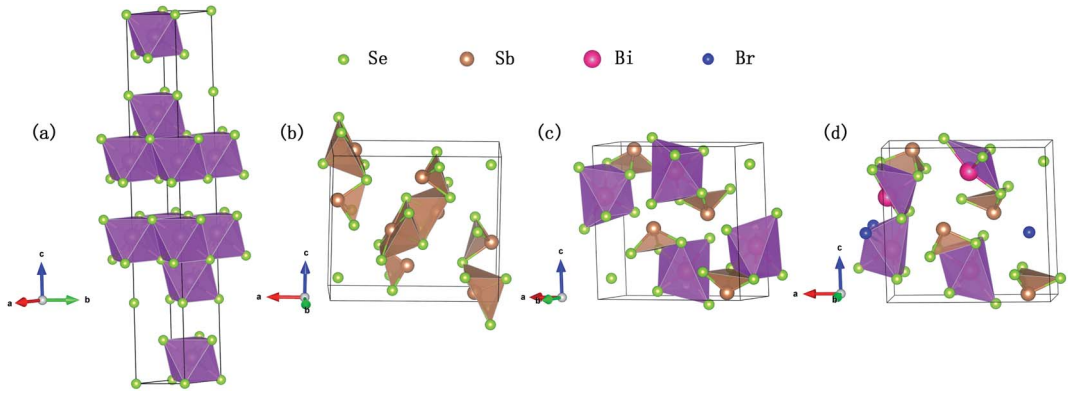

Fig. 1 Crystal structure of Bi_2Se_3 (a), Sb_2Se_3 (b), $BiSbSe_3$ (c), and $BiSb(Se_{0.92}Br_{0.08})_3$ (d), with Bi, Sb, Se, and Br atoms shown as red, brown, green, and blue spheres, respectively.

results are qualitatively similar. Herein, we take the lowest energy structure with Se3 replaced by Br atom to model the $BiSb(Se_{0.92}Br_{0.08})_3$.

As shown in Fig. 1(d), this structure also possesses a stable orthorhombic structure (space group *Pnma*) but is more complex: not only an octahedral structure with Bi atom as the center and Se atom as the apex, and a triangular pyramidal tetrahedron with one Sb and three Se atoms as the apex are formed, but also formed is an octahedral structure with Bi as the center and both Se and Br atoms as the vertices. This more complex structure may be helpful to further suppressing the lattice thermal conductivity.

The conduction band and valence band model can be used to analyze how the carrier concentration and the band gap affect the TE properties. The calculated electronic band structures of $Bi_{2-x}Sb_x(Se_{1-y}Br_y)_3$ ($x = 0, 1, 2; y = 0, 0.08$) are shown in Fig. 2. It is worth mentioning that the band structures of $Bi_{2-x}Sb_x(Se_{1-y}Br_y)_3$ ($x = 1, 2; y = 0, 0.08$) are given by the TB-mBJ functional, while those of Bi_2Se_3 (band gap ~ 0.17 eV) is given by the PBE-GGA functional so that we can have a direct comparison with a previous PBE-GGA result ($\sim$0.16 eV), as shown in Table 1.

One can see in Table 1 that the previous PBE-GGA result of the E_g of Sb_2Se_3 ($\sim$0.7 eV) is largely underestimated with respect to the experimental value ($\sim$1.17 eV), while our TB-mBJ result ($\sim$1.11 eV) is in good agreement. In order to ensure the accuracy of the calculated results, we use TB-mBJ to calculate the band structures of $Bi_{2-x}Sb_x(Se_{1-y}Br_y)_3$ ($x = 1, 2; y = 0, 0.08$). The SOC are considered in our calculations due to the heavy element. As can be seen in Table 1 and Fig. 2, the $Bi_{2-x}Sb_x(Se_{1-y}Br_y)_3$ ($x = 1, 2; y = 0, 0.08$) have much larger band gaps than Bi_2Se_3, which can largely suppress the intrinsic excitation and the bipolar effect to prevent them from reaching a higher zT value. In addition, the 8% Br codoping further makes the Fermi level (E_F) shifted to deeper conduction states, indicating that the Br codoping increases significantly the majority carrier concentration.

As is well known, a large N_v is beneficial to a large DOS effective mass (m^*_{DOS}) without deterioration of the carrier mobility μ.[4,39] N_v is the effective total number of independent carrier pockets or valleys in the Brillouin zone, including both symmetry and orbital degeneracies. For Bi_2Se_3, it can be seen that alloying 50% Sb on Bi sites increases the valley number of effective energy from the degeneracy 2 to 10. As one can see in

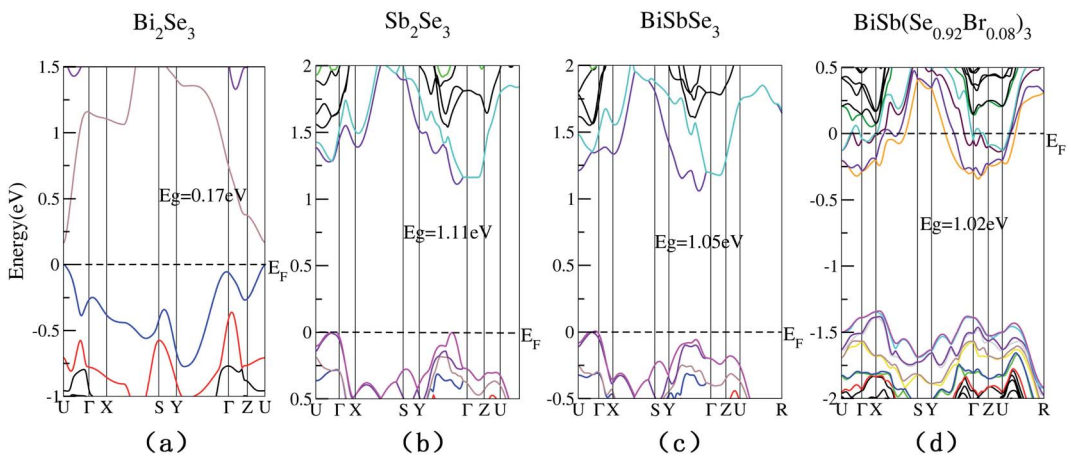

Fig. 2 Calculated electronic band structures of Bi_2Se_3 (a), Sb_2Se_3 (b), $BiSbSe_3$ (c), and $BiSb(Se_{0.92}Br_{0.08})_3$ (d).

Table 1 Lattice parameters and band gaps of $Bi_{2-x}Sb_x(Se_{1-y}Br_y)_3$ ($x = 0, 1, 2$; $y = 0, 0.08$)

	Experimental value				Previously calculated value				Our calculated value			
Compounds	a	b	c	E_g	a	b	c	E_g	a	b	c	E_g
Bi_2Se_3	4.14[a]	4.14[a]	28.63[a]	0.25[a]	4.17[a]	4.17[a]	30.29[a]	0.16[a]	4.19	4.19	30.80	0.17
Sb_2Se_3	11.77[b]	3.96[b]	11.62[b]	1.17[b]	11.53[b]	3.96[b]	11.22[b]	0.75[b]	12.82	4.03	11.53	1.11
$BiSbSe_3$	11.70[c]	3.91[c]	11.62[c]	0.88[c]	12.59[c]	4.10[c]	11.65[c]	0.63[c]	12.63	4.10	11.62	1.05
$BiSb(Se_{0.92}Br_{0.08})_3$	10.52[d]	5.26[d]	10.17[d]	—	11.84[d]	4.07[d]	11.67[d]	—	12.36	4.16	11.65	1.02

[a] Result from ref. 27. [b] Result from ref. 28. [c] Result from ref. 29. [d] Result from ref. 23.

Fig. 2(c), the energy difference between the CBM and the fourth valence valley is less than ~0.14 eV, which is smaller than the 0.15 eV between the first and the second valence bands of PbTe.[40] Such small energy difference can be easily crossed at elevated temperatures, making it possible to improve the electrical transport properties. Furthermore, 8% Br subsequent codoping at Se12 position exhibits remarkably distinct electronic structures, which further significantly increases the effective N_v, accompanied by pushing the E_F deep into the band structure, which significantly enlarges the n. A high N_v number generally results in a larger m^*_{DOS} for the conduction band and eventually maintains a high S for n-type samples in spite of the increased n. Interestingly, the conduction bands of $BiSb(Se_{0.92}Br_{0.08})_3$ are much more complex than those of $BiSbSe_3$: the activated multiple conduction-band minima lie close together in energy, forming complex multiband valence states. Another illustration of the complex band structure is shown in the Fermi surface, which has multiple types of valleys coming from the four conduction bands of E_F crossing, all within a small energy window (see Fig. 3(a)–(d)). Such a good band feature may be associated with excellent thermoelectric properties, as found in other thermoelectric materials.[39,41]

To clearly understand the states near the E_F, we calculate the total density of states (TDOS) for Bi_2Se_3, $BiSbSe_3$, and $BiSb(Se_{0.92}Br_{0.08})_3$ respectively, as shown in Fig. 4(a). It should be noted that TDOS near the Fermi level of doped Bi_2Se_3 is larger than that of pristine Bi_2Se_3. 50% Sb doping on Bi sites of Bi_2Se_3 slightly increased the TDOS near the E_F. This is mainly originated from the substitution of Sb for Bi, which increases N_v. Furthermore, 8% Br codoping at Se12 site in $BiSbSe_3$ tremendously increases the TDOS in the vicinity of the E_F, which will enhance σ significantly. These results manifest that Sb and Br dual doped Bi_2Se_3 can be expected to have enhanced electrical transport and thermoelectric properties. To analyze the reasons for the enhanced TDOS by Br substitution, we calculate the partial density of states (PDOS) of $BiSb(Se_{0.92}Br_{0.08})_3$. As can be seen in Fig. 4(b), the bottom of CB edge is mainly contributed by the hybridized p orbitals from Bi, Se, Br, and Sb atoms (see the next section for more details). Thus, the Br atom replacement on the Se12 site can effectively adjust the band structure near the CB edge, and strongly enhances the thermoelectric performance.

Bonding properties

To visualize the electronic environments and bonding conditions, charge density difference (CDD) is calculated for $BiSb(Se_{0.92}Br_{0.08})_3$ compound. Fig. 4(c) reveals that the negative electron density is mainly around atoms Bi and Sb, meaning overall Bi and Sb atoms donate their valence electrons to the $[Se_{0.92}Br_{0.08}]_3^{2-}$. The electronegativity on the Pauling scale for

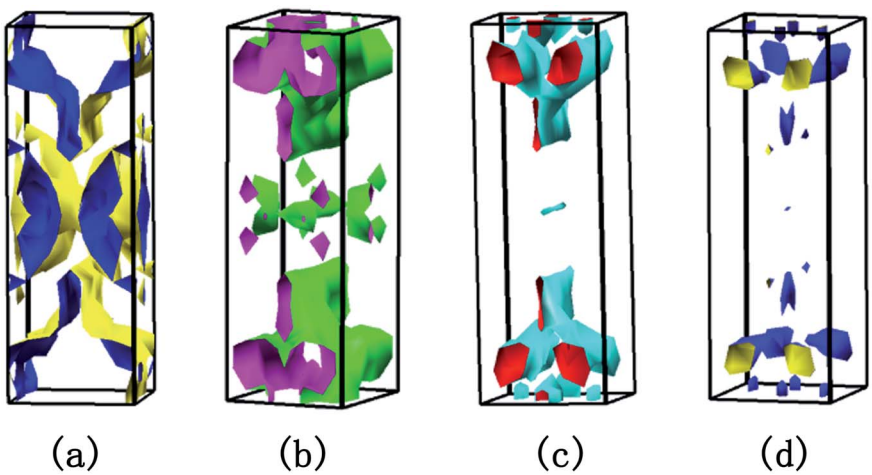

Fig. 3 The energy isosurfaces at 0.37 eV of $BiSb(Se_{0.92}Br_{0.08})_3$ (space group: *Pnma*, no. 62). (a), (b), (c) and (d) are the four conduction bands traversed by Fermi level from bottom to top, respectively.

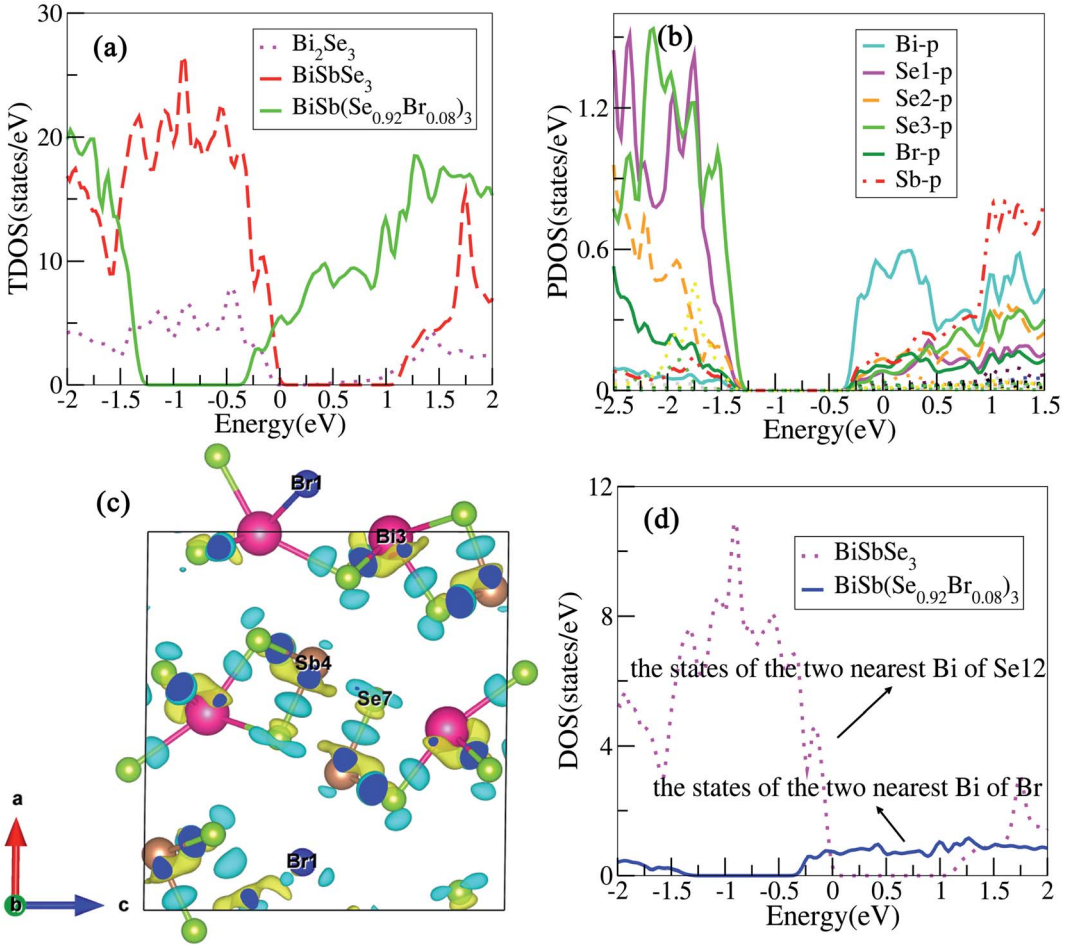

Fig. 4 (a) Calculated the TDOS of Bi_2Se_3, $BiSbSe_3$, and $BiSb(Se_{0.92}Br_{0.08})_3$. (b) and (c) are the PDOS, the charge density difference of $BiSb(Se_{0.92}Br_{0.08})_3$, respectively. The colors yellow and cyan in (c) represent the negative and positive charge differences, respectively. (d) Projected density of states on the two nearest Bi atoms of Se12 and Br.

Bi, Sb, Se and Br are 2.02, 2.05, 2.55, and 2.96, respectively. The electropositive elements Bi and Sb dedicate all of their valence electrons to the more electronegative elements Se and Br, ultimately, $BiSb(Se_{0.92}Br_{0.08})_3$ can be described as $(BiSb)^{3+}(Se_{0.92}Br_{0.08})_3^{2-}$. It coincides with the above analysis that, in $BiSb(Se_{0.92}Br_{0.08})_3$, Bi and Sb atoms tend to lose electrons, while Se and Br atoms tend to gain electrons owing to their larger electronegativity. These also manifest that Br–Bi has a stronger interaction than Se–Bi. In fact, the stronger hybridization between Br and Bi atoms will conduce to increasing the DOS near the CB edge, as indicated in Fig. 4(d). The electrons between the Bi and Br atoms mainly localizes around Br, while a certain number of electrons appear around the center position between Bi and Se, and Sb and Se atoms, indicating Bi and Br atoms incline to form an ionic bond, while there is a distinct covalent bond characteristics between Bi and Se, and Sb and Se atoms. The ionicity of the bonding in a material usually is characterized by the electronegativity difference ($\Delta\chi$). The larger $\Delta\chi$ ($\approx$0.9 between Br and Bi atoms), the more likely there will be interaction between carriers and the optical vibrations of the lattice atoms,[42] thus suppressing the κ_L. For instance, observations by Ioffe *et al.* showed a decrease of κ with an increase of the ionicity of the bonds between atoms.[42] Spitzer reported a correlation between increasing coordination number (CN) in a crystal structure and decreasing κ_L (by relating the κ_L to the strength of the chemical bonds in a material).[42] In our case, the bond lengths between atoms after Br codoping become longer, namely, Se12–Bi bond lengths (2.81, 3.12 Å) in the $BiSbSe_3$ are shorter than the corresponding Br–Bi bond lengths (3.05, 3.23 Å) in $BiSb(Se_{0.92}Br_{0.08})_3$. This implies that the Br–Bi bond could be relatively weaker according to the bonding descriptor contact developed by Deringer *et al.*[28] The weaker chemical bond among Br and Bi atoms will be also a factor leading to the low κ_L (see the next section), as also recognized recently in α-MgAgSb.[43] In addition, the big "mushroom" CDD shape around Bi/Sb is a clear indicator of the existence of lone-pair electrons, which is alike to the case of $CuSbS_2$.[44] According to the valence shell electron pair repulsion (VSEPR) theory,[45] the lone-pair electrons almost occupy one bonding site. Hence, the unsymmetrical and disorderly coordinated environment of bonds in $BiSb(Se_{0.92}Br_{0.08})_3$ indicates the possibility of strong

anharmonicity by significantly enhancing heat carrying phonon scatterings. This will also result in ultralow κ_L.

Low lattice thermal conductivities

To achieve a high thermoelectric figure of merit, a low lattice thermal conductivity is essential. Therefore, insights into the origin of the extremely low thermal conductivity is meaningful for exploiting high performance thermoelectric materials. Previous work predicted that $BiSbSe_3$ could possess a low κ_L.[23] Nevertheless, the prediction was based on a strong dependence of the elastic properties on volume, and the resulting large Grüneisen parameter (γ, an indicator of anharmonicity) suggests a strong anharmonicity. In this work, we precisely calculate the κ_L as a function of temperature for $BiSbSe_3$ and $BiSb(Se_{0.92}Br_{0.08})_3$ using the full linearized ShengBTE code combined with DFT, which is well known for quantitative predictive power.[46] The results are presented in Fig. 5.

As mentioned previously, the substitution of Sb for 50% Bi in Bi_2Se_3 decreases the κ_L partly due to the structural phase transition from rhombohedral to orthorhombic, and partly due to the formation of the more complex chain-like structure with respect to the layered structure, which induces enhanced intrinsic phonon scatterings. In Fig. 5 our *ab initio* results are compared with the experimental κ_L values of polycrystalline samples cited from ref. 23. It is worth mentioning that the calculated values are averaged over the three principal axes for the purpose of better vision and comparison with the experimental measurements on polycrystalline samples. It can be seen that the predicted values of $BiSbSe_3$ are below 1.2 W m^{-1} K^{-1} at 300 K, which is pretty low in thermoelectric materials.[47,48] However, the experimental values are even much lower at low temperatures though the agreement between theory and experiment is improved at high temperatures. The large discrepancy in κ_L at low temperatures may not be entirely attributed to grain boundary scattering, since this effect is usually small in materials with intrinsically low κ_L, where heat carrying phonons have smaller mean free paths than the size of the grains.[49,50] It has to be noted that the theoretical calculation does not take into account the phonon scattering due to dynamic disorder, an omission that may be responsible for the overestimation of κ_L.

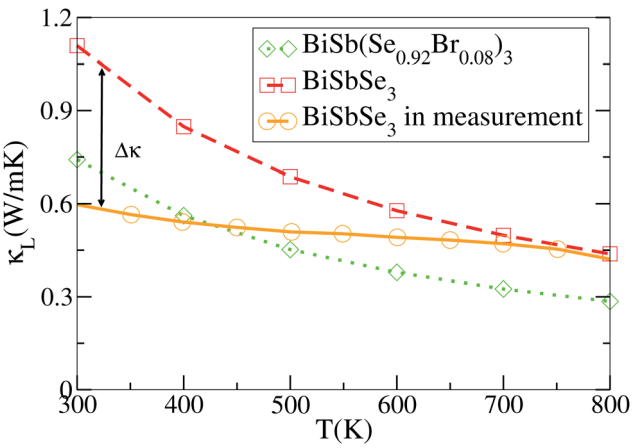

Fig. 5 Experimental and DFT-calculated lattice thermal conductivities as functions of temperature.

Here a possible mechanism is that the underlying atomic disorder plays an appreciable role in reducing κ_L at relatively low temperatures. While at high temperatures atoms occupy higher-symmetry positions,[51] and intrinsic phonon–phonon scattering then dominates, as described by Eivari *et al.*[55] For example, the previously mentioned lone-pair electrons may provide an origination of thus disorder which can act as a phonon-blocking mechanism that may help facilitate an ultralow κ_L. Moreover, we find that 8% Br codoping is also effective to further reduce κ_L as shown in Fig. 5. $BiSb(Se_{0.92}Br_{0.08})_3$ shows a lower κ_L than that of $BiSbSe_3$ at the entire temperature. For instance, their κ_L are 0.29 and 0.44 W m^{-1} K^{-1} at 800 K, respectively. Clearly, the chemical bond softening between Br and Bi atoms is considerably higher than that between Se12 and Bi. As we know, the strong anharmonicity usually not only relies directly on the unsymmetrical and chemical bonds between the atoms in the crystal but also is often associated with atoms and their near neighbors (large coordination numbers). The calculated κ_L of $BiSb(Se_{0.92}Br_{0.08})_3$ is found to be in good agreement with an available experimental value 0.22 W m^{-1} K^{-1} at 800 K.[23]

Promising electrical transport properties

To shed light on the influences of Sb–Br codoping, herein the electrical transport properties of $BiSbSe_3$ and $BiSb(Se_{0.92}Br_{0.08})_3$ are calculated as functions of carrier concentration (n) at 300 K, 600 K, and 800 K within the framework of the semiclassical Boltzmann transport theory.[52] While it is possible to calculate σ/τ as a function of n and T, but it is not possible to calculate σ itself without the scattering rate τ^{-1}. Here, the strategy previously used by Ong *et al.*[53] is adopted with available experimental data[23] to estimate the relaxation time $\tau = C_0 T^{-1} n^{-1/3}$ with τ in s, T in K, and n in cm^{-3}. The specific details are that we used 800 °C data from Liu and coworkers,[23] who made measurements on the material. They report a thermopower $S = -202.462$ μV K^{-1} at this temperature. By comparing with the calculated $S(T, n)$, we obtain a value $n = 1.77 \times 10^{20}$ cm^{-3} for this sample. The reported experimental σ is 172.899 S cm^{-1}, which combined with the calculated σ/τ yields $\tau = 2.345 \times 10^{-15}$ s for this particular sample at 800 °C. As mentioned, we then calculate σ as $\sigma/\tau \times \tau$. Ultimately, the results for $BiSbSe_3$ and $BiSb(Se_{0.92}Br_{0.08})_3$ are plotted in Fig. 6.

Based on the estimated τ, we can calculate the κ_e using the BoltzTraP2 code. Unfortunately, with the significant increase of n, the κ_e augments from ~0.05 W m^{-1} K^{-1} of $BiSbSe_3$ at 300 K, to ~0.34 W m^{-1} K^{-1} of $BiSb(Se_{0.92}Br_{0.08})_3$ at 800 K. However, as discussed previously, Br codoping notably reduces the κ_L from ~1.11 W m^{-1} K^{-1} at 300 K to ~0.29 W m^{-1} K^{-1} at 800 K. Therefore, a favorable κ (~0.63 W m^{-1} K^{-1}) could still be obtained for $BiSb(Se_{0.092}Br_{0.08})_3$ at 800 K. Then, by combining the calculated κ_L, κ_e, S, and σ of $BiSbSe_3$ and $BiSb(Se_{0.92}Br_{0.08})_3$, we determine their zTs at different temperatures and carrier concentrations. Fascinatingly, compared with 50% Sb doped

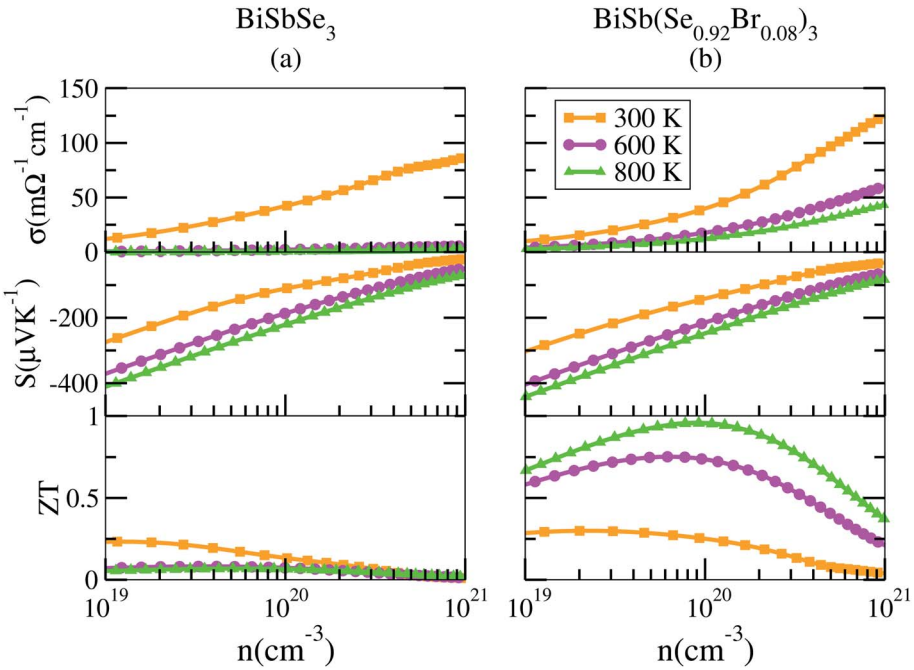

Fig. 6 Calculated transport properties of n-type $BiSbSe_3$ (a), and $BiSb(Se_{0.92}Br_{0.08})_3$ (b), respectively.

$BiSbSe_3$ (maximum $zT \sim 0.23$ with the optimal n of 1.163×10^{19} cm^{-3} at 800 K, see Fig. 6(a)), further 8% Br codoping enhances σ, hence strikingly improves the zT (maximum ~ 0.96 with the optimal n of 9.224×10^{19} cm^{-3} at 800 K, see Fig. 6(b)). $BiSb(Se_{0.92}Br_{0.08})_3$ exhibits a still high S that may originate from the increase of m^*_{DOS} owing to the increase of N_v through Br codoping. On the other hand, the remarkably enhanced σ shown in Fig. 6(b) may originate from the increases of n and/or μ.

To show this more clearly, we calculate n and μ as functions of temperature for $BiSbSe_3$ and $BiSb(Se_{0.92}Br_{0.08})_3$, as depicted in Fig. 7. μ is obtained from the calculated σ and n by using the expression $\mu = \sigma/ne$. One can see that, 8% Br codoping dramatically enlarges n, and in the meantime, μ is still promoted at medium high temperatures. The significant increase of n in $BiSb(Se_{0.92}Br_{0.08})_3$ is essentially due to the one more electron of Br atom with respect to Se. Thus, Br atom acts as an electron donor though it has a large electronegativity. Consequently, the E_F shifts deeper in the CB and the differential conductivity turns into more symmetric regarding the Fermi level.[54] Our Bader charge analyses show consistently that each nearest neighbor Bi atom of Br averagely obtains more 0.44 electrons from the Br atom than that from Se. In addition, the hybridization of the electronic states then provides a large DOS around the Fermi level, as already shown in Fig. 4(d). A direct result is the remarkably enhanced σ. However, the dramatically increased n in the Sb–Br codoping system does not significantly reduce the S: it is -261.93 μV K^{-1} for $BiSbSe_3$ at 300 K and -254.12 μV K^{-1} for $BiSb(Se_{0.92}Br_{0.08})_3$ at 800 K. Based on the aforementioned data and analyses, this explicit increase is most likely due to the N_v augment, which is the key parameter for making a compromise between n and S. Normally, the optimum n for most good TE materials is in the range of 10^{19} to 10^{21} cm^{-3}. Optimization of the carrier concentration is still one of the most effective approaches for improving TE performance. Especially, in the case of some TE materials with intrinsically low thermal conductivity, a high zT can be obtained solely through doping.

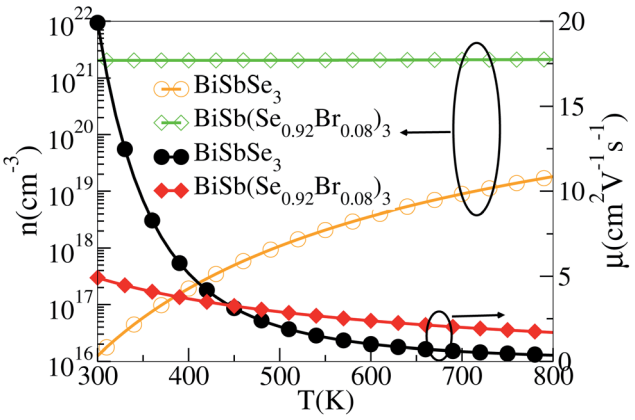

Fig. 7 Calculated n and μ of $BiSb(Se_{0.92}Br_{0.08})_3$ as functions of temperature.

Methods

First-principles calculations

The atomic structures of $Bi_{2-x}Sb_x(Se_{1-y}Br_y)_3$ ($x = 0, 1, 2$; $y = 0$, 0.08) are optimized utilizing the plane-wave projector augmented wave (PAW) method[24] as implemented in the Vienna *ab initio* simulation package (VASP)[25] based on DFT. The

Perdew–Burke–Ernzerhof parametrization of the generalized gradient approximation (PBE-GGA) is used for the exchange–correlation potential. The wave function is expanded using plane waves with a kinetic energy cutoff of 400 eV. A $(5 \times 15 \times 5)$ Monkhorst–Pack[26] k-point mesh is used for the Brillouin zone (BZ) sampling. The spin–orbit coupling (SOC) is considered in all the calculations due to the heavy element. The geometry optimization is performed for every Br doping configuration by relaxing both atomic positions and lattice constants. The energy convergence criterion is chosen to be 10^{-7} eV. The Hellmann–Feynman forces on each ion are less than 0.001 eV $Å^{-1}$. The residual stress is set to be less than 0.1 GPa. Here, we discuss only the configuration with the lowest total energy. The calculated lattice constants are listed in Table 1. These values agree well with previous results reported in literature.[23,27–29]

The electronic structures of $Bi_{2-x}Sb_x(Se_{1-y}Br_y)_3$ ($x = 0, 1, 2$; $y = 0, 0.08$) are then calculated using the linearized augmented plane wave (LAPW) method,[30] as implemented in the WIEN2k code.[31] The muffin-tin radii (RMT) are set to 2.5, 2.46, 2.46, and 2.5 a.u. for Bi, Sb, Se, and Br, respectively. The cutoff parameter $RMT \times K_{max} = 9$ (K_{max} is the magnitude of the largest k vector) is used. The self-consistent DFT calculations are performed with a $(5 \times 15 \times 5)$ k-point mesh in the irreducible BZ, and the total energy is converged to within 0.0001 Ry. Since the local or semilocal exchange–correlation approximation underestimates band gaps as the presence of artificial self-interaction and the absence of the derivative discontinuity in the exchange–correlation functional,[32] band gaps with better accuracy are calculated using the Tran–Blaha modified Becke–Johnson (TB-mBJ) functional.[33] The calculated electronic structures with the TB-mBJ functional are further used to obtain electrical transport properties. The transport calculations are carried out using the semiclassical Boltzmann theory, as implemented in the BoltzTraP code[34] within the constant scattering time approximation, by taking 20 000 k points in the irreducible BZ.

The lattice thermal conductivity can be determined by using an iterative self-consistent method for solving the phonon Boltzmann transport equation as implemented in the ShengBTE code.[35,36] The harmonic lattice dynamics and the second-order interatomic force constants (IFCs) are determined by the density functional perturbation theory (DFPT)[37] implemented in VASP with a supercell of $1 \times 3 \times 1$ and the PHONOPY code[38] interfaced to VASP. The third-order anharmonic IFCs are extracted from the DFT calculations by applying the finite displacement method with a supercell of $1 \times 3 \times 1$ and a truncation for next–nearest–neighbor interactions up to the tenth order. As for the k-point sampling of the BZ, our test calculations adopting a $1 \times 3 \times 1$ and a $3 \times 3 \times 3$ k-point mesh show that the thermal conductivities are converged very well. In this work, a $3 \times 3 \times 3$ mesh is used for all the supercell calculations.

Summary and conclusion

In this work, we performed comprehensive investigations of both the thermal and electrical transport properties of $BiSbSe_3$ and $BiSb(Se_{0.92}Br_{0.08})_3$ by using first-principles calculations combined with the Boltzmann transport theory. The results demonstrate that the dual doping of Sb–Br in Bi_2Se_3 leads to both low κ_L and promising electrical transport properties. First, the chemical bond softening between Br and Bi atoms and lone-pair electrons act as a phonon-blocking mechanism which greatly suppresses κ_L with strong anharmonicity. Second, the one more electron of Br atom with respect to Se makes the Br atom acts as an electron donor, which dramatically increases the carrier concentration n in $BiSb(Se_{0.92}Br_{0.08})_3$. As a result, the DOS near the E_F is significantly increased and more conduction bands participate in the electron transport, leading to a remarkably enhanced σ. Third, the 8% Br subsequent codoping exhibits remarkably distinct electronic structures and transport properties, which further significantly increases the effective N_v. This multiple degeneracy of conduction band edges is a distinctive feature of $BiSb(Se_{0.92}Br_{0.08})_3$, enabling an extraordinary high PF by giving rise to a large m^*_{DOS} and thus preserving a large S in spite of the dramatically increased n. Combined with the low κ and excellent electrical transport properties, the n-type $BiSb(Se_{0.92}Br_{0.08})_3$ presents an outstanding thermoelectric performance, especially around 800 K: the maximum zT can reach 0.96 with the optimal n of 9.224×10^{19} cm^{-3}. This work shows theoretically the possibility for crystalline materials to achieve a high thermoelectric performance without introducing defects and/or nanostructures, and provides a possible guidance and inspiration for seeking new promising Te-free thermoelectric materials.

Data availability

The data that support the findings of this study are available from corresponding author upon reasonable request.

Author contributions

S.-H. Ke conceived the idea. J. Zhang conducted the simulation and analysis. S. Zhong provided advices on this work. All authors participated in the writing and correction of the manuscript.

Conflicts of interest

The authors declare no competing interests.

Acknowledgements

This work was supported by the Natural Science Foundation of Shanghai under Grant No. 19ZR1459100 and by the National Natural Science Foundation of China under Grant No. 11374226.

References

1 L. D. Zhao, S. H. Lo, Y. Zhang, H. Sun, G. Tan, C. Uher, C. Wolverton, V. P. Dravid and M. G. Kanatzidis, Ultralow Thermal Conductivity and High Thermoelectric Figure of Merit in SnSe Crystals, *Nature*, 2014, **508**, 373.

2 Y. Wu, F. Liu, Q. Zhang, T. Zhu, K. Xia and X. Zhao, Enhancing the Average Thermoelectric Figure of Merit of Elemental Te by Suppressing Grain Boundary Scattering, *J. Mater. Chem. A*, 2020, **8**, 8455.

3 X. Zhang, C. Liu, Y. Tao, Y. Li, Y. Guo, Y. Chen, X. C. Zeng and J. Wang, High ZT 2D Thermoelectrics by Design: Strong Interlayer Vibration and Complete Band-Extrema Alignment, *Adv. Funct. Mater.*, 2020, **30**, 2001200.

4 Y. Xiao, D. Wang, Y. Zhang, C. Chen, S. Zhang, K. Wang, G. Wang, S. J. Pennycook, G. J. Snyder, H. Wu, *et al.*, Band Sharpening and Band Alignment Enable High Quality Factor to Enhance Thermoelectric Performance in n-Type PbS, *J. Am. Chem. Soc.*, 2020, **142**, 4051.

5 Z. Wei, C. Wang, J. Y. Zhang, J. Yang and J. Luo, Precise Regulation of Carrier Concentration in Thermoelectric BiSbTe Alloys via Magnetic Doping, *ACS Appl. Mater. Interfaces*, 2020, **12**, 20653–20663.

6 L. Xi, S. Pan, X. Li, Y. Xu, J. Ni, X. Sun, J. Yang, J. Luo, J. Xi, W. Zhu, *et al.*, Discovery of High-Performance Thermoelectric Chalcogenides through Reliable High-Throughput Material Screening, *J. Am. Chem. Soc.*, 2018, **140**, 10785.

7 S. Wang, L. Su, Y. Qiu, Y. Xiao and L. D. Zhao, Enhanced Thermoelectric Performance in Cl-doped $BiSbSe_3$ with Optimal Carrier Concentration and Effective Mass, *Am. J. Mater. Sci. Technol.*, 2020, **70**, 67.

8 Z. Z. Luo, S. Cai, S. Hao, T. P. Bailey, I. Spanopoulos, Y. Luo, J. Xu, C. Uher, C. Wolverton, V. P. Dravid, *et al.*, Inducing Strong Valence Band Convergence to Enhance Thermoelectric Performance in PbSe with Two Chemically Independent Knobs, *Angew. Chem., Int. Ed.*, 2020, **132**, 2.

9 S. Q. Lin, W. Li, Z. L. Bu, B. Shan and Y. Z. Pei, Thermoelectric p-Type Ag_9GaTe_6 with an Intrinsically Low Lattice Thermal Conductivity, *ACS Appl. Energy Mater.*, 2020, **3**, 1892.

10 H. J. Goldsmid, Thermoelectric Refrigeration, *Electr. Eng.*, 2013, **79**, 380.

11 F. J. Disalvo, Thermoelectric Cooling and Power Generation, *Science*, 1999, **285**, 703.

12 P. Yanzhong, S. Xiaoya, A. LaLonde, W. Heng, C. Lidong, *et al.*, Convergence of Electronic Bands for High Performance Bulk Thermoelectrics, *Nature*, 2011, **473**, 66.

13 W. Qiu, L. Xi, P. Wei, X. Ke and W. Zhang, Part-Crystalline Part-Liquid State and Rattling-Like Thermal Damping in Materials with Chemical-Bond Hierarchy, *Proc. Natl. Acad. Sci. U. S. A.*, 2014, **111**, 15031.

14 S. Wang, J. Yang, L. Wu, P. Wei, J. Yang, W. Zhang and Y. Grin, Anisotropic Multicenter Bonding and High Thermoelectric Performance in Electron-Poor CdSb, *Chem. Mater.*, 2015, **27**, 1071.

15 K. Peng, X. Lu, H. Zhan, S. Hui, X. Tang, G. Wang, J. Dai, C. Uher, G. Wang and X. Zhou, Broad Temperature Plateau for High ZTs in Heavily Doped p-Type SnSe Single Crystals, *Energy Environ. Sci.*, 2016, **9**, 454.

16 L. Hu, H. Wu, T. Zhu, C. Fu, J. He, P. Ying and X. Zhao, Tuning Multiscale Microstructures to Enhance Thermoelectric Performance of n-Type Bismuth-Telluride-Based Solid Solutions, *Adv. Energy Mater.*, 2015, **5**, 1500411.

17 Y. X. Yang, Y. H. Wu, Q. Zhang, G. S. Cao and X. B. Zhao, Enhanced Thermoelectric Performance of Bi_2Se_3/TiO_2 Composite, *Rare Met.*, 2020, **8**, 887–894.

18 W. Liu, K. Lukas, K. Mcenaney, S. Lee, Q. Zhang, C. Opeil, G. Chen and Z. Ren, Studies on the Bi_2Te_3-Bi_2Se_3-Bi_2S_3 System for Mid-Temperature Thermoelectric Energy Conversion, *Energy Environ. Sci.*, 2013, **6**, 552.

19 W. Zhang, R. Yu, H. Zhang, X. Dai and Z. Fang, First-Principles Studies of the Three-Dimensional Strong Topological Insulators Bi_2Te_3, Bi_2Se_3 and Sb_2Te_3, *New J. Phys.*, 2010, **12**, 065013.

20 Y. Min, J. W. Roh, H. Yang, M. Park, I. K. Sang, S. Hwang, M. L. Sang, K. H. Lee and U. Jeong, Surfactant-Free Scalable Synthesis of Bi_2Te_3 and Bi_2Se_3 Nanoflakes and Enhanced Thermoelectric Properties of Their Nanocomposites, *Adv. Mater.*, 2012, **25**, 1425.

21 Y. Pei, H. Wang and G. J. Snyder, Band Engineering of Thermoelectric Materials, *Adv. Mater.*, 2012, **24**, 6125.

22 S. Wang, Y. Sun, J. Yang, B. Duan, L. Wu, W. Zhang and J. Yang, High Thermoelectric Performance in Te-free $(Bi,Sb)_2Se_3$ via Structural Transition Induced Band Convergence and Chemical Bond Softening, *Energy Environ. Sci.*, 2016, **9**, 3436.

23 X. Liu, D. Wang, H. Wu, J. Wang, Y. Zhang, G. Wang, S. J. Pennycook and L. D. Zhao, Intrinsically Low Thermal Conductivity in $BiSbSe_3$: A Promising Thermoelectric Material with Multiple Conduction Bands, *Adv. Funct. Mater.*, 2018, **29**, 1806558.

24 P. E. Blöchl, Projector Augmented-Wave Method, *Phys. Rev. B: Condens. Matter Mater. Phys.*, 1994, **50**, 17953.

25 G. Kresse and J. Furthmuller, Efficiency of Ab Initio Total Energy Calculations for Metals and Semiconductors Using a Plane-Wave Basis Set, *Comput. Mater. Sci.*, 1996, **6**, 15.

26 H. J. Monkhorst and J. D. Pack, Special Points for Brillouin-Zone Integrations, *Phys. Rev. B: Solid State*, 1976, **13**, 5188.

27 B. T. Wang and P. Zhang, Phonon Spectrum and Bonding Properties of Bi_2Se_3: Role of Strong Spin-Orbit Interaction, *Appl. Phys. Lett.*, 2012, **100**, 146401.

28 V. L. Deringer, R. P. Stoffel, M. Wuttig and R. Dronskowski, Vibrational Properties and Bonding Nature of Sb_2Se_3 and Their Implications for Chalcogenide Materials, *Chem. Sci.*, 2015, **6**, 5255.

29 Z. Zhang, R. Zhang, N. Qi, Y. Wu and Z. Chen, Microscopic Origin of the Extremely Low Thermal Conductivity and Outstanding Thermoelectric Performance of $BiSbX_3$ (X = S, Se) Revealed by First-Principles Study, *Phys. Chem. Chem. Phys.*, 2020, **22**, 15559.

30 E. SjöStedt, L. NordströM and D. J. Singh, An Alternative Way of Linearizing the Augmented Plane-Wave Method, *Solid State Commun.*, 2000, **114**, 15.

31 R. Nityananda, P. Hohenberg and W. Kohn, Inhomogeneous Electron Gas, *Resonance*, 2017, **22**, 809.

32 L. J. Sham and M. Schlüter, Density-Functional Theory of the Energy Gap, *Phys. Rev. Lett.*, 1983, **51**, 1888.

33 F. Tran and P. Blaha, Accurate Band Gaps of Semiconductors and Insulators with a Semilocal Exchange-Correlation Potential, *Phys. Rev. Lett.*, 2009, **102**, 226401.

34 A. F. May, E. S. Toberer, A. Saramat and G. J. Snyder, Characterization and Analysis of Thermoelectric Transport in n-Type $Ba_8Ga_{16-x}Ge_{30+x}$, *Phys. Rev. B: Condens. Matter Mater. Phys.*, 2009, **80**, 125205.

35 W. Li, J. Carrete, N. A. Katcho and N. Mingo, ShengBTE: A Solver of the Boltzmann Transport Equation for Phonons, *Comput. Phys. Commun.*, 2014, **185**, 1747.

36 W. Li, N. Mingo, L. Lindsay, D. A. Broido, D. A. Stewart and N. A. Katcho, Thermal Conductivity of Diamond Nanowires from First Principles, *Phys. Rev. B: Condens. Matter Mater. Phys.*, 2012, **85**, 195436.

37 S. Baroni, S. de Gironcoli, A. Dal Corso and P. Giannozzi, Phonons and Related Crystal Properties from Density-Functional Perturbation Theory, *Rev. Mod. Phys.*, 2001, **73**, 515.

38 A. Togo, F. Oba and I. Tanaka, First-Principles Calculations of the Ferroelastic Transition Between Rutile-Type and $CaCl_2$-type SiO_2 at High Pressures, *Phys. Rev. B: Condens. Matter Mater. Phys.*, 2008, **78**, 134106.

39 Z. Feng, X. Zhang, Y. Wang, J. Zhang, T. Jia, B. Cao and Y. Zhang, Thermoelectric Optimization of $AgBiSe_2$ by Defect Engineering for Room-Temperature Applications, *Phys. Rev. B*, 2019, **99**, 155203.

40 L. D. Zhao, G. Tan, S. Hao, J. He, Y. Pei, H. Chi, H. Wang, S. Gong, H. Xu and V. P. Dravid, Ultrahigh Power Factor and Thermoelectric Performance in Hole-Doped Single-Crystal SnSe, *Science*, 2015, **351**, 141.

41 J. Zhang, X. Zhang and Y. Wang, Hf/Sb Co-Doping Induced a High Thermoelectric Performance of ZrNiSn: First-principles Calculation, *Sci. Rep.*, 2017, **7**, 14590.

42 W. G. Zeier, A. Zevalkink, Z. M. Gibbs, G. Hautier, M. G. Kanatzidis and G. J. Snyder, Thinking Like a Chemist: Intuition in Thermoelectric Materials, *Angew. Chem., Int. Ed.*, 2016, **55**, 6826.

43 P. Ying, X. Li, Y. Wang, J. Yang, C. Fu, W. Zhang, X. Zhao and T. Zhu, Hierarchical Chemical Bonds Contributing to the Intrinsically Low Thermal Conductivity in alpha-MgAgSb Thermoelectric Materials, *Adv. Funct. Mater.*, 2017, **27**, 1604145.

44 Z. Feng, T. Jia, J. Zhang, Y. Wang and Y. Zhang, Dual Effects of Lone-Pair Electrons and Rattling Atoms in $CuBiS_2$ on Its Ultralow Thermal Conductivity, *Phys. Rev. B*, 2017, **96**, 235205.

45 R. J. Gillespie and R. S. Nyholm, Inorganic Stereochemistry, *Q. Rev., Chem. Soc.*, 1957, **11**, 339.

46 T. Jia, J. Carrete, Z. Feng, S. Guo, Y. Zhang and G. K. H. Madsen, Localized Dimers Drive Strong Anharmonicity and Low Lattice Thermal Conductivity in ZnSe2, *Phys. Rev. B*, 2020, **102**, 125204.

47 K. Xia, Y. Liu, S. Anand, G. J. Snyder, J. Xin, J. Yu, X. Zhao, X. B. Zhao and T. Zhu, Enhanced Thermoelectric Performance in 18-Electron $Nb_{0.8}CoSb$ Half-Heusler Compound with Intrinsic Nb Vacancies, *Adv. Funct. Mater.*, 2018, **28**, 1705845.

48 Z. Ma, J. Wei, P. Song, M. Zhang, L. Yang, J. Ma, W. Liu, F. Yang and X. Wang, Review of Experimental Approaches for Improving zT of Thermoelectric Materials, *Mater. Sci. Semicond. Process.*, 2021, **121**, 105303.

49 L. D. Zhao, C. Chang, G. Tan and M. G. Kanatzidis, SnSe: a Remarkable New Thermoelectric Material, *Energy Environ. Sci.*, 2016, **9**, 3044.

50 J. M. Hodges, Y. Xia, C. D. Malliakas, G. C. B. Alexander, M. K. Y. Chan and M. G. Kanatzidis, Two-Dimensional $CsAg_5Te_{3-x}S_x$ Semiconductors: Multi-anion Chalcogenides with Dynamic Disorder and Ultralow Thermal Conductivity, *Chem. Mater.*, 2018, **30**, 7245–7254.

51 M. T. Dove, Theory of Displacive Phase Transitions in Minerals, *Am. Mineral.*, 1997, **82**, 213.

52 G. K. H. Madsen, J. Carrete and M. J. Verstraete, BoltzTraP2, a Program for Interpolating Band Structures and Calculating Semi-Classical Transport Coefficients, *Comput. Phys. Commun.*, 2017, **231**, 140.

53 K. P. Ong, D. J. Singh and P. Wu, Analysis of the Thermoelectric Properties of n-type ZnO, *Phys. Rev. B*, 2011, **83**, 115110.

54 T. Zhu, Y. Liu, C. Fu, J. P. Heremans, J. G. Snyder and X. Zhao, Compromise and Synergy in High-Efficiency Thermoelectric Materials, *Adv. Mater.*, 2017, **29**, 1605884.

55 H. A. Eivari, Z. Sohbatzadeh, P. Mele and M. H. N. Assadi, Low thermal conductivity: fundamentals and theoretical aspects in thermoelectric applications, *Mater. Today Energy*, 2021, **21**, 100744.

56 J. J. G. Moreno, J. Cao, M. Fronzi and M. H. N. Assadi, A review of recent progress in thermoelectric materials through computational methods, *Mater. Renew. Sustain. Energy*, 2020, **9**, 16.

57 A. Shakouri, Recent Developments in Semiconductor Thermoelectric Physics and Materials, *Annu. Rev. Mater. Res.*, 2011, **41**, 399–431.